High Resolution Spectroscopy of $^{12}_{\Lambda}$B by Electroproduction

M. Iodice,[1] F. Cusanno,[2] A. Acha,[3] P. Ambrozewicz,[3] K. A. Aniol,[4] P. Baturin,[5] P. Y. Bertin,[6] H. Benaoum,[7]
K. I. Blomqvist,[8] W. U. Boeglin,[9] H. Breuer,[9] P. Brindza,[10] P. Bydžovský,[11] A. Camsonne,[6] C. C. Chang,[9] J.-P. Chen,[10]
Seonho Choi,[12] E. A. Chudakov,[10] E. Cisbani,[13] S. Colilli,[13] L. Coman,[3] B. J. Craver,[14] G. De Cataldo,[15] C. W. de Jager,[10]
R. De Leo,[15] A. P. Deur,[14] C. Ferdi,[6] R. J. Feuerbach,[10] E. Folts,[10] R. Fratoni,[13] S. Frullani,[13] F. Garibaldi,[13] O. Gayou,[16]
F. Giulani,[13] J. Gomez,[10] M. Gricia,[13] J. O. Hansen,[10] D. Hayes,[17] D. W. Higinbotham,[10] T. K. Holmstrom,[18]
C. E. Hyde,[17,6] H. F. Ibrahim,[17] X. Jiang,[5] L. J. Kaufman,[19] K. Kino,[20] B. Kross,[10] L. Lagamba,[15] J. J. LeRose,[10]
R. A. Lindgren,[14] M. Lucentini,[13] D. J. Margaziotis,[4] P. Markowitz,[3] S. Marrone,[15] Z. E. Meziani,[12] K. McCormick,[5]
R. W. Michaels,[10] D. J. Millener,[21] T. Miyoshi,[22] B. Moffit,[18] P. A. Monaghan,[16] M. Moteabbed,[3] C. Muñoz Camacho,[23]
S. Nanda,[10] E. Nappi,[15] V. V. Nelyubin,[14] B. E. Norum,[14] Y. Okasyasu,[22] K. D. Paschke,[19] C. F. Perdrisat,[18] E. Piasetzky,[24]
V. A. Punjabi,[25] Y. Qiang,[16] B. Raue,[3] P. E. Reimer,[26] J. Reinhold,[3] B. Reitz,[10] R. E. Roche,[27] V. M. Rodriguez,[28]
A. Saha,[10] F. Santavenere,[13] A. J. Sarty,[29] J. Segal,[10] A. Shahinyan,[30] J. Singh,[14] S. Širca,[31] R. Snyder,[14] P. H. Solvignon,[12]
M. Sotona,[11] R. Subedi,[32] V. A. Sulkosky,[18] T. Suzuki,[22] H. Ueno,[33] P. E. Ulmer,[17] G. M. Urciuoli,[2] P. Veneroni,[13]
E. Voutier,[34] B. B. Wojtsekhowski,[10] Y. Ye,[35] X. Zheng,[26] S. Zhou,[36] and C. Zorn[10]

(Jefferson Lab Hall A Collaboration)

[1]*Istituto Nazionale di Fisica Nucleare, Sezione di Roma Tre, I-00146 Roma, Italy*
[2]*Istituto Nazionale di Fisica Nucleare, Sezione di Roma1, Piazza Aldo Moro, Rome, Italy*
[3]*Florida International University, Miami, Florida 33199, USA*
[4]*California State University, Los Angeles, Los Angeles, California 90032, USA*
[5]*Rutgers, The State University of New Jersey, Piscataway, New Jersey 08855, USA*
[6]*Université Blaise Pascal/IN2P3, F-63177 Aubière, France*
[7]*Syracuse University, Syracuse, New York 13244, USA*
[8]*Universität Mainz, Mainz, Germany*
[9]*University of Maryland, College Park, Maryland 20742, USA*
[10]*Thomas Jefferson National Accelerator Facility, Newport News, Virginia 23606, USA*
[11]*Nuclear Physics Institute, Řež near Prague, Czech Republic*
[12]*Temple University, Philadelphia, Pennsylvania 19122, USA*
[13]*Istituto Nazionale di Fisica Nucleare, Sezione di Roma1, gruppo collegato Sanità, and Istituto Superiore di Sanitá, I-00161 Roma, Italy*
[14]*University of Virginia, Charlottesville, Virginia 22904, USA*
[15]*Istituto Nazionale di Fisica Nucleare, Sezione di Bari and University of Bari, I-70126 Bari, Italy*
[16]*Massachussets Institute of Technology, Cambridge, Massachusetts 02139, USA*
[17]*Old Dominion University, Norfolk, Virginia 23508, USA*
[18]*College of William and Mary, Williamsburg, Virginia 23187, USA*
[19]*University of Massachusetts Amherst, Amherst, Massachusetts 01003, USA*
[20]*Research Center for Nuclear Physics, Osaka University, Ibaraki, Osaka 567-0047, Japan*
[21]*Brookhaven National Laboratory, Upton, New York 11973, USA*
[22]*Tohoku University, Sendai, 980-8578, Japan*
[23]*CEA Saclay, DAPNIA/SPhN, F-91191 Gif-sur-Yvette, France*
[24]*School of Physics and Astronomy, Sackler Faculty of Exact Science, Tel Aviv University, Tel Aviv 69978, Israel*
[25]*Norfolk State University, Norfolk, Virginia 23504, USA*
[26]*Argonne National Laboratory, Argonne, Illinois 60439, USA*
[27]*Florida State University, Tallahassee, Florida 32306, USA*
[28]*University of Houston, Houston, Texas 77204, USA*
[29]*St. Mary's University, Halifax, Nova Scotia, Canada*
[30]*Yerevan Physics Institute, Yerevan, Armenia*
[31]*Department of Physics, University of Ljubljana, Slovenia*
[32]*Kent State University, Kent, Ohio 44242, USA*
[33]*Yamagata University, Yamagata 990-8560, Japan*
[34]*LPSC, Université Joseph Fourier, CNRS/IN2P3, INPG, F-38026 Grenoble, France*
[35]*University of Science and Technology of China, Hefei, Anhui, China*
[36]*China Institute of Atomic Energy, Beijing, China*

An experiment measuring electroproduction of hypernuclei has been performed in hall A at Jefferson Lab on a ^{12}C target. In order to increase counting rates and provide unambiguous kaon identification two superconducting septum magnets and a ring imaging Cherenkov detector were added to the hall A standard equipment. An unprecedented energy resolution of less than 700 keV FWHM has been achieved. Thus, the observed $^{12}_\Lambda$B spectrum shows for the first time identifiable strength in the core-excited region between the ground-state s-wave Λ peak and the 11 MeV p-wave Λ peak.

Hypernuclei, long-lived baryonic systems with strangeness $\neq 0$, provide us with a variety of nuclear phenomena. For example, a Λ hyperon (baryon with strangeness $S = -1$ and mean lifetime $\tau \sim 10^{-10}$ s) can be placed deep inside the nucleus as an impurity providing a sensitive probe of the nuclear interior. The Λ couples weakly to nuclear core states and the $V_{N\Lambda}$ residual interaction removes the degeneracy of the multiplets. In the case of a Λ in an s orbit, the resulting doublet is split by the spin-dependent components of the interaction. The doublet spacings range from a few up to several hundred keV. Since very limited information can be obtained from elementary hyperon-nucleon scattering, hypernuclei are unique laboratories for studying the ΛN interaction.

In the past, hypernuclear spectroscopy has been carried out with limited resolution by means of hadronic reactions, such as the strangeness-exchange $^{A}Z(K^-, \pi^-)^{A}_\Lambda Z$ and associated-production $^{A}Z(\pi^+, K^+)^{A}_\Lambda Z$ reactions. More recently, γ-ray spectroscopy has been used to measure hypernuclear transition energies. Here, the few-keV energy resolution has allowed precise level assignments and the measurement of doublet spacings [1] but the method is limited to the bound region below particle emission thresholds and to bound levels reached following particle emission.

The experimental knowledge can be enhanced using electroproduction of strangeness that is characterized by a large 3-momentum transfer to the hypernucleus ($\gtrsim 250$ MeV/c), a large angular momentum transfer ΔJ, and strong spin-flip terms, even at zero kaon production angle. Moreover, the $K^+\Lambda$ pair production occurs on a proton in contrast to a neutron in (K^-, π^-) or (π^+, K^+) reactions making possible the study of different hypernuclei and charge-dependent effects from a comparison of mirror hypernuclei.

The E94-107 experiment in hall A at Jefferson Lab [2] (JLab) started a systematic study of high-resolution hypernuclear spectroscopy on p-shell targets, specifically ^{9}Be, ^{12}C, and ^{16}O. The results on ^{12}C are presented in this Letter.

^{12}C targets have been extensively used in hypernuclear studies with the (K^-, π^-), (π^+, K^+), and $(K^-_{\text{stop}}, \pi^-)$ reactions that are dominated by non-spin-flip contributions. In the early experiments, only two peaks, attributed to the Λ in s or p orbits coupled to the ^{11}C ground state, were evident [1]. The first evidence of structure between the main peaks came from (π^+, K^+) studies with the SKS

spectrometer at KEK (E140a, E336, and E369) [1], with the best resolution of 1.45 MeV in KEK E369 [3]. Recently, in the stopped K^- experiment of the FINUDA Collaboration [4], further evidence for structure in this region has been observed. The first electroproduction experiment [5] performed on a ^{12}C target at JLab in hall C had limited statistics but proved that the electroproduction process can be used to study hypernuclear spectra with sub-MeV energy resolution and measured cross sections.

Hall A at JLab is well suited to perform $(e, e'K^+)$ experiments. Scattered electrons can be detected in the high-resolution spectrometer (HRS) electron arm while coincident kaons are detected in the HRS hadron arm [6]. The disadvantage of smaller electromagnetic cross sections is partially compensated for by the high current, high duty cycle, and high energy resolution capabilities of the beam at Jefferson Lab. In the present experiment, a 100 mg/cm^2 ^{12}C target was used with an electron beam current of 100 μA.

The strong inverse dependence of the cross section on Q^2, squared virtual photon 4-momentum transfer, calls for measurements at low Q^2. To maximize the cross section, the electron scattering angle must be minimized, subject to avoiding the increasing background from processes at very forward electron angles. To minimize the momentum transferred to the hypernucleus, and maximize the cross section, a detection angle θ_K for the K^+ must be chosen near the virtual photon direction. The high beam energy results in a relatively high momentum for the kaon, as required to keep a reasonable survival fraction in the spectrometer (25 m flight path). So, kinematics were set to particle detection at 6° for both electrons and kaons, incident beam energy of 3.77 GeV, scattered electron momentum of 1.56 GeV/c, and kaon momentum of 1.96 GeV/c.

In order to allow experiments at forward angles smaller than the HRS's minimum angle (12.5°), a superconducting septum magnet was added to each HRS. Particles at scattering angles of 6° are deflected by the septum magnets into the HRS. This new spectrometer configuration (septum + HRS) provides a general purpose device that extends the HRS features to small scattering angles while preserving the spectrometer optical performance [7]. The energy resolution depends on the momentum resolution of the HRS spectrometers, on the straggling and energy loss in the target, and on the beam energy spread. A momentum resolution of the system (HRS's + septum magnets) of

$\Delta p/p = 10^{-4}$ (FWHM) and a beam energy spread as small as 6×10^{-5} (FWHM) are necessary to be able to achieve an excitation-energy resolution of about 500 keV. With a dedicated effort the accelerator staff were able to address the beam quality requirements and to set up new devices for continuous beam energy spread monitoring.

The high background level demands a very efficient PID system with unambiguous kaon identification. The standard PID system in the hadron arm is composed of two aerogel threshold Cherenkov counters [6,8] ($n_1 = 1.015$, $n_2 = 1.055$). Charged pions (protons) with momenta around 2 GeV/c are above (below) the Cherenkov light emission threshold. Kaons emit Cherenkov light only in the $n_2 = 1.055$ detector. Hence, a combination of the signals from the two counters should distinguish among the three species of hadrons. However, due to inefficiencies and delta-ray production, the identification of kaons has contamination from pions and protons. This has driven the design, construction, and installation of a Ring Imaging Cherenkov (RICH) detector, conceptually identical to the ALICE HMPID design [9], in the hadron HRS detector package. It uses a proximity focusing geometry, a cesium iodide photocathode, and a 15 mm thick liquid perfluorohexane radiator. A detailed description of the layout and the performance of the RICH detector is given in [10–12]. In the electron arm, the gas Cherenkov counters give pion rejection ratios up to 10^3. The remaining background (due to knock-on electrons) is reduced by a further 2 orders of magnitude by the lead glass preshower and shower counters, giving a total pion rejection ratio of 10^5.

The essential role of the RICH in identifying kaons is shown in Fig. 1, where the unfilled, without RICH, should be compared to the filled spectrum, with RICH. All contributions from pions and protons completely vanish with the RICH.

In Fig. 2, the excitation-energy spectrum of $^{12}_{\Lambda}$B is shown for the full range of energy acceptance. The filled histogram shows the low level of $(e, e') \otimes (e, K^+)$ random coincidence background. Figure 3 shows the sixfold differential cross section expressed in nb/(sr^2 GeV MeV). The background has been evaluated by fitting the data obtained for random coincidences in a large timing window. No residual background in the negative range of E_x is present after subtraction. The origin of the excitation-energy scale has been set to the peak value of the ground-state (g.s.) level (the uncertainty of the absolute scale being about 0.5 MeV).

The first step in fitting the data was to use a peak search algorithm [13] to identify six regions with an excess of counts above background at the 90% confidence level. When fitted with Gaussian functions, individual peaks show non-Gaussian contributions, mainly in the tails due to the radiative effects. Voigt functions [14], convolutions of Gaussian with Lorentzian functions, are often used in spectroscopy to better fit the data. The main idea in fitting the data is to minimize the number of assumptions. Since each peak might contain a more complex (unresolved) structure, each Voigt function allows the width, location, and height to vary independently. The best fit is thus determined by minimizing χ^2/n.d.f. with respect to the positions, widths, and amplitudes of 6 Voigt functions and parameters of the quasifree region modeled by a quadratic form. The results of the parameters obtained in the fit with χ^2/n.d.f. = 1.16, together with the statistical significance of the assigned levels [in terms of SNR = signal/$\sqrt{\text{(signal + background)}}$] and cross sections, as obtained after a radiative unfolding procedure, are given in Table I.

The narrowest width of 670 ± 150 keV has been measured for the peak at $E_x = 10.93$ MeV, indicating that the
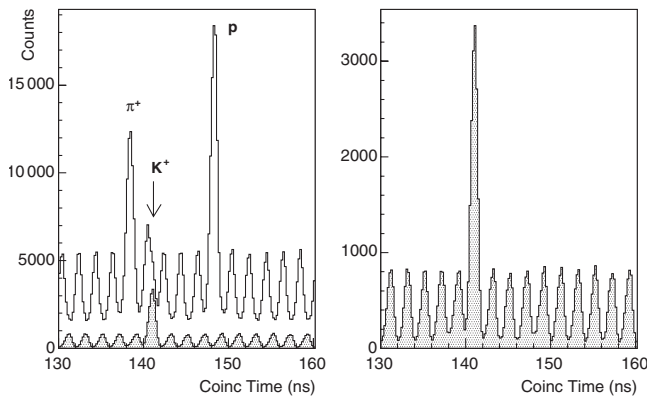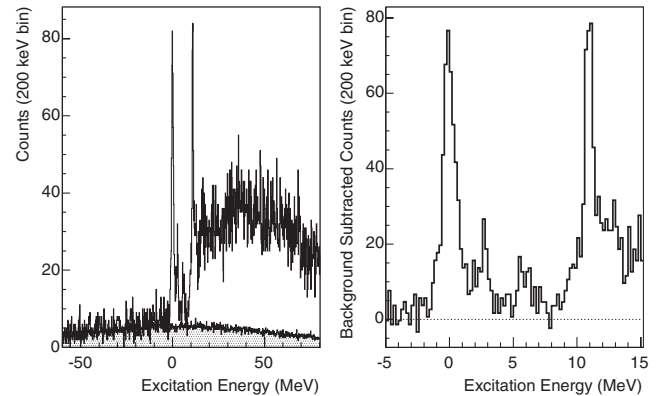

FIG. 1.   Hadron plus electron arm coincidence time spectra. In the left panel, the unfilled histogram is obtained by selecting kaons with only the threshold aerogel Cherenkov detectors. The filled histogram (expanded in the right panel) includes the RICH kaon selection. The remaining contamination is due to accidental $(e, e') \otimes (e, K^+)$ coincidences.

FIG. 2.   The $^{12}_{\Lambda}$B excitation-energy spectrum obtained after kaon selection with aerogel detectors and RICH. The electron-kaon random coincidence contribution evaluated in a large timing window is superimposed on the spectrum in the left panel. The right panel shows the spectrum after this background has been subtracted.

TABLE I. Levels and cross sections obtained by fitting the ^{12}C$(e, e'K^+)^{12}_{\Lambda}$B spectrum compared with theoretical predictions. In column 6, p_{Λ} for the 1^+ states indicates strongly mixed $p_{1/2}$ and $p_{3/2}$ configurations.

Experimental data				Theoretical prediction			
Position (MeV)	Width (FWHM, MeV)	SNR	Cross section (nb/sr^2/GeV)	E_x (MeV)	Main structure	J^{π}	Cross section (nb/sr^2/GeV)
0.0 ± 0.03	1.15 ± 0.18	19.7	4.48 ± 0.29(stat) ± 0.63(syst)	0.0	^{11}B$(\frac{3}{2}^-; \text{g.s.}) \otimes s_{1/2\Lambda}$	1^-	1.02
				0.14	^{11}B$(\frac{3}{2}^-; \text{g.s.}) \otimes s_{1/2\Lambda}$	2^-	3.66
2.65 ± 0.10	0.95 ± 0.43	7.0	0.75 ± 0.16(stat) ± 0.15(syst)	2.67	^{11}B$(\frac{1}{2}^-; 2.12) \otimes s_{1/2\Lambda}$	1^-	1.54
5.92 ± 0.13	1.13 ± 0.29	5.3	0.45 ± 0.13(stat) ± 0.09(syst)	5.74	^{11}B$(\frac{3}{2}^-; 5.02) \otimes s_{1/2\Lambda}$	2^-	0.58
				5.85	^{11}B$(\frac{3}{2}^-; 5.02) \otimes s_{1/2\Lambda}$	1^-	0.18
9.54 ± 0.16	0.93 ± 0.46	4.4	0.63 ± 0.20(stat) ± 0.13(syst)	…	…	…	…
10.93 ± 0.03	0.67 ± 0.15	20.0	3.42 ± 0.50(stat) ± 0.55(syst)	10.48	^{11}B$(\frac{3}{2}^-; \text{g.s.}) \otimes p_{3/2\Lambda}$	2^+	0.24
				10.52	^{11}B$(\frac{3}{2}^-; \text{g.s.}) \otimes p_{\Lambda}$	1^+	0.12
				10.98	^{11}B$(\frac{3}{2}^-; \text{g.s.}) \otimes p_{1/2\Lambda}$	2^+	1.43
				11.05	^{11}B$(\frac{3}{2}^-; \text{g.s.}) \otimes p_{3/2\Lambda}$	3^+	2.19
12.36 ± 0.13	1.58 ± 0.29	7.3	1.19 ± 0.36(stat) ± 0.35(syst)	12.95	^{11}B$(\frac{1}{2}^-; 2.12) \otimes p_{3/2\Lambda}$	2^+	0.91
				13.05	^{11}B$(\frac{1}{2}^-; 2.12) \otimes p_{\Lambda}$	1^+	0.27

experimental excitation-energy resolution is at least compatible with this value.

On the other hand, the width for the g.s. peak, around $E_x = 0.0$ MeV, is 1150 ± 180 keV, wider than 670 keV, although, within errors, not in sharp statistical disagreement.

Such a larger width might suggest a more complex structure underlying the g.s. peak. The possibility of an unresolved doublet has been explored by fitting with two Voigt functions, constraining their widths to be the same as the peak at $E_x = 10.93$ MeV. The result is that the separation between the two Voigt shapes is about 650 keV, larger than the 140 keV predicted by the theory. However, with the present sample of data, there is not enough statistical significance to favor such a result over a simple statistical fluctuation of the widths. This situation could be clarified either with a larger sample of data or by an improvement in the experimental resolution.

Because of the very low level of background, states with an s_{Λ} coupled to excited ^{11}B core states are clearly observed between the g.s. and the level at 10.93 MeV with signal to noise ratios (SNR) larger than 5. The positions of these levels can be determined with uncertainties less than 150 keV. Cross sections are determined at the level of 15%–20%.

In Fig. 3, the measured electroproduction cross sections for hypernuclear states are also compared with a model (dashed line), which shows very good overall agreement with the data without any normalization factor. The theoretical cross sections were obtained in the framework of the distorted wave impulse approximation (DWIA) [15] using the Saclay-Lyon (SLA) model [16] for the elementary

$p(e, e'K^+)\Lambda$ reaction. Shell-model wave functions for ^{11}B and $^{12}_{\Lambda}$B were obtained using fitted p-shell interactions and a parametrization of the ΛN interaction that fits the precise γ-ray spectra of $^{7}_{\Lambda}$Li [17]. The results are compared with experiment in Table I.

The large g.s. peak and another strong peak at ~ 10.93 MeV correspond to the substitution of a p-shell proton by a Λ in s and p states, respectively, coupled dominantly to the $3/2^-$ g.s. of ^{11}B. Two peaks at $E_x = 2.65$ MeV and $E_x = 5.92$ MeV are also evident. Theoretically (see Table I), they should be due to the 1^- member of the 0^-, 1^- doublet based on the $1/2^-$ state of ^{11}B at $E_x = 2.125$ MeV and to the 1^-, 2^- doublet based on the $3/2^-$ level of ^{11}B at $E_x = 5.020$ MeV, with the domi-

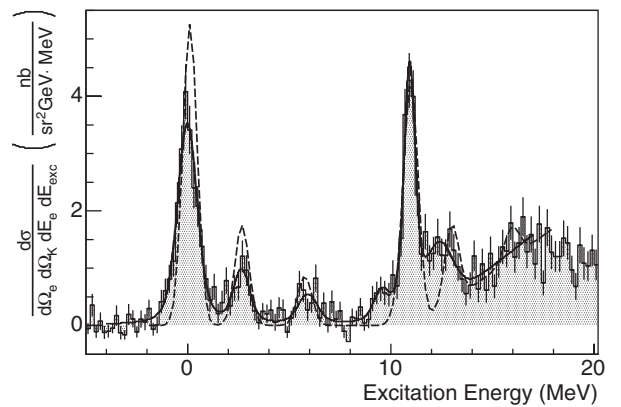FIG. 3. The $^{12}_{\Lambda}$B excitation-energy spectrum. The best fit (solid curve) and a theoretical prediction (dashed curve) are superimposed on the data. See text for details.

nant contribution coming from the 2^- state. The raising of the doublet energies relative to the unperturbed core energies is mainly due to the $\vec{l}_{N\Lambda} \cdot \vec{s}_N$ component of the effective ΛN interaction [18]. The energies and cross sections for the three s_Λ peaks are well reproduced by the theoretical predictions for the five s_Λ states.

Because the Λ spin-orbit interaction is weak, the calculation predicts essentially degenerate 2^+ and 3^+ states from $^{11}\mathrm{B}(3/2^-) \otimes p_\Lambda$ coupling. Table I shows that these two states dominate in the main peak observed close to 11 MeV. There is clearly strength on either side of this peak, accounted for in the fit by peaks at 9.54 MeV (though at the limit of statistical significance) and at 12.36 MeV. The theoretical p_Λ strength based on the ground and first-excited states of $^{11}\mathrm{B}$ accounts for 98% of the observed strength. There are six known positive-parity states between 9 and 12 MeV in $^{11}\mathrm{B}$ [19] to which an s_Λ can couple to form 2^+ or 3^+ hypernuclear states. Based on existing $(e, e'p)$ data, these states are expected to be only weakly excited and an admixture with the nearby p_Λ states is required for them to be excited as strongly as observed in the present data. From their shell-model structure, the 9.88 MeV $3/2^+$ and 11.60 MeV $5/2^+$ states of $^{11}\mathrm{B}$ should be the most important but a full $1\hbar\omega$ shell-model calculation is needed to investigate this problem.

In summary, a high-quality, background-free $^{12}_{\Lambda}\mathrm{B}$ hypernuclear spectrum with unprecedented energy resolution (~ 670 keV) has been obtained. The new experimental devices have proven to be very effective. In particular, septum magnets had no adverse affect on the HRS optics and the RICH played an essential role in the unambiguous identification of kaons.

The measured cross section for the g.s. doublet is in very good agreement with the value of 4.68 nb/sr^2/GeV predicted using the SLA model. The s_Λ part of the spectrum is well reproduced by the theory and a very good agreement is also obtained for the other levels. For the first time a measurable strength with good energy resolution has been observed in the core-excited part of the spectrum. This is helped by the fact that the spin-spin interaction enhances these states with respect to the weak-coupling limit. The distribution of strength within several MeV on either side of the strong p_Λ peak should stimulate theoretical work to better understand the p_Λ region.

[1] O. Hashimoto and H. Tamura, Prog. Part. Nucl. Phys. **57**, 564 (2006).
[2] F. Garibaldi, S. Frullani, P. Markowitz, and J. LeRose, spokespersons, J Lab Experiment E94-107, High Resolution $1p$ shell Hypernuclear Spectroscopy, 1994.
[3] H. Hotchi *et al.*, Phys. Rev. C **64**, 044302 (2001).
[4] M. Agnello *et al.*, Phys. Lett. B **622**, 35 (2005).
[5] T. Miyoshi *et al.*, Phys. Rev. Lett. **90**, 232502 (2003); L. Yuan *et al.*, Phys. Rev. C **73**, 044607 (2006).
[6] J. Alcorn *et al.*, Nucl. Instrum. Methods Phys. Res., Sect. A **522**, 294 (2004).
[7] G. M. Urciuoli *et al.*, Nucl. Phys. **A691**, 43c (2001).
[8] L. Lagamba *et al.*, Nucl. Instrum. Methods Phys. Res., Sect. A **471**, 325 (2001).
[9] ALICE Collaboration, HMPID TDR, CERN/LHCC98-19, 1998.
[10] M. Iodice *et al.*, Nucl. Instrum. Methods Phys. Res., Sect. A **553**, 231 (2005).
[11] F. Garibaldi *et al.*, Nucl. Instrum. Methods Phys. Res., Sect. A **502**, 117 (2003).
[12] F. Cusanno *et al.*, Nucl. Instrum. Methods Phys. Res., Sect. A **502**, 251 (2003).
[13] Y. Qiang *et al.*, Phys. Rev. C **75**, 055208 (2007).
[14] B. H. Armstrong, J. Quant. Spectrosc. Radiat. Transfer **7**, 61 (1967).
[15] M. Sotona and S. Frullani, Prog. Theor. Phys. Suppl. **117**, 151 (1994).
[16] T. Mizutani, C. Fayard, G.-H. Lamot, and B. Saghai, Phys. Rev. C **58**, 75 (1998).
[17] M. Ukai *et al.*, Phys. Rev. C **73**, 012501(R) (2006).
[18] D. J. Millener, Nucl. Phys. **A691**, 93c (2001).
[19] F. Ajzenberg-Selove, Nucl. Phys. **A506**, 1 (1990).